

Search for the Signatures of a New-Born Black Hole from the Collapse of a Supra-massive Millisecond Magnetar in Short GRB Light Curves

Q. Zhang,^{1*} W. H. Lei,² B. B. Zhang^{3,4} W. Chen,² S. L. Xiong,¹ and L. M. Song¹

¹Key Laboratory of Particle Astrophysics, Institute of High Energy Physics, Chinese Academy of Sciences, Beijing 100049, China

²School of Physics, Huazhong University of Science and Technology, Wuhan 430074, China

³Instituto de Astrofísica de Andalucía (IAA-CSIC), P.O. Box 03004, E-18080 Granada, Spain

⁴Scientist Support LLC, Madsion, AL 35758, USA

Accepted XXX. Received YYY; in original form ZZZ

ABSTRACT

‘Internal plateau’ followed by a sharp decay is commonly seen in short gamma-ray burst (GRB) light curves. The plateau component is usually interpreted as the dipole emission from a supra-massive magnetar, and the sharp decay may imply the collapse of the magnetar to a black hole (BH). Fall-back accretion onto the new-born BH could produce long-lasting activities via the Blandford-Znajek (BZ) process. The magnetic flux accumulated near the BH would be confined by the accretion disks for a period of time. As the accretion rate decreases, the magnetic flux is strong enough to obstruct gas infall, leading to a magnetically-arrested disk (MAD). Within this scenario, we show that the BZ process could produce two types of typical X-ray light curves: type I exhibits a long-lasting plateau, followed by a power-law decay with slopes ranging from 5/3 to 40/9; type II shows roughly a single power-law decay with slope of 5/3. The former requires low magnetic field strength, while the latter corresponds to relatively high values. We search for such signatures of the new-born BH from a sample of short GRBs with an internal plateau, and find two candidates: GRB 101219A and GRB 160821B, corresponding to type II and type I light curve, respectively. It is shown that our model can explain the data very well.

Key words: accretion, accretion disks – gamma-ray burst: individual (GRB 101219A, GRB 160821B) – stars: black holes – stars: magnetars

1 INTRODUCTION

Short gamma-ray bursts (GRBs), with durations typically less than 2 s (Kouveliotou et al. 1993), have been widely speculated to be produced by mergers of two compact objects: either a double neutron star or a neutron star (NS) and a black hole (BH) binary (Eichler et al. 1989; Paczynski 1991; Narayan, Paczynski & Piran 1992). This is observationally supported by their host galaxy properties, the locations of the bursts in the host galaxies, as well as non-detection of supernova associations (e.g., Barthelmy et al. 2005b; Berger et al. 2005; Fox et al. 2005; Gehrels et al. 2005; Fong et al. 2010; Kann et al. 2011; Berger 2014). While NS-BH mergers inevitably end up in a BH instantly, NS-NS mergers can result in different types of remnants. Depending on the total mass of the NS-NS system and the NS equation of state (EOS), the final products of NS-NS merg-

ers could be a prompt BH¹, a supra-massive NS (SMNS) temporarily supported by uniform rotation and collapses to a BH until the centrifugal force is insufficient to support the mass, or a stable NS (e.g., Rosswog & Davies 2002; Giacomazzo & Perna 2013; Ravi & Lasky 2014; Ciolfi et al. 2017).

The discovery of $\sim 2M_{\odot}$ NSs suggests that the EOS is stiff enough for SMNSs to be created from the merger of two NSs (Demorest et al. 2010; Antoniadis et al. 2013; Hebel et al. 2013). Moreover, observations of the early afterglows of a large sample of short GRBs with *Swift* show rich features that indicate extended engine activities, such as extended emission (Norris & Bonnell 2006),

¹ Here ‘prompt BH’ means that the merger product may either immediately collapse to a BH or survive for ~ 10 – 100 ms as a hypermassive neutron supported by strong differential rotation and thermal pressures (e.g., Baiotti et al. 2008; Kiuchi et al. 2009; Rezzolla et al. 2011; Hotokezaka et al. 2013).

* E-mail: zhangqiang@ihep.ac.cn

X-ray flares (Barthelmy et al. 2005b; Campana et al. 2006; Margutti et al. 2011) and X-ray plateaus (Rowlinson et al. 2013; Lü et al. 2015). These features are hard to interpret within the framework of a BH central engine, but are compatible with a rapidly spinning, strongly magnetized NS or ‘millisecond magnetar’ as the central engine (e.g., Dai et al. 2006; Gao & Fan 2006; Metzger, Quataert & Thompson 2008; Rowlinson et al. 2010, 2013; Gompertz et al. 2013; Gompertz, O’Brien & Wynn 2014).

A good fraction of short GRBs detected with *Swift* show ‘internal X-ray plateaus’ within the first few hundred seconds, followed by a sharp drop with a temporal decay index of $\alpha > 3^2$, sometimes approaching $\alpha \sim 10$ (Rowlinson et al. 2010, 2013; Lü et al. 2015). Such an internal plateau has also been observed in several long GRBs (Troja et al. 2007; Lyons et al. 2010; Lü & Zhang 2014), but they are commonly observed in short GRBs. This kind of plateau, followed by a rapid decay which is too steep to be explained within the external shock model, can be interpreted as the internal emission of the magnetar wind, and the sharp decay marks the abrupt cessation of the central engine, likely due to the collapse of a supra-massive magnetar to a BH (Troja et al. 2007; Rowlinson et al. 2010; Zhang 2013, 2014). Since the GRB outflow still produces X-ray afterglow by the external shock during the internal plateau phase, it is expected to emerge once the X-ray emission from the magnetar wind drops below the external component. This has been seen clearly in several X-ray afterglows of both long and short GRBs (Troja et al. 2007; Lyons et al. 2010; Rowlinson et al. 2013; Lü & Zhang 2014; Lü et al. 2015; De Pasquale et al. 2016; Zhang, Huang & Zong 2016). The external component typically shows a power-law (PL) decay with slope of ~ 1 which is consistent with the prediction of the standard afterglow models (Sari, Piran & Narayan 1998; Chevalier & Li 2000).

Nevertheless, the recent observed GRB 160821B seems to challenge the above scenario. GRB160821B is a nearby bright short GRB detected by *Swift* and *Fermi* (Siegel et al. 2016; Stanbro & Meegan 2016), with a redshift of $z = 0.16$ (Levan et al. 2016). Its X-ray afterglow exhibits an internal plateau lasting for ~ 180 s, then drops steeply with a slope of ~ 4.5 . About 1000 s after the Burst Alert Telescope (BAT; Barthelmy et al. 2005a) trigger, another plateau component emerges, which lasts for $\sim 3 \times 10^4$ s with a decay slope of ~ 0.45 , then the light curve declines with a slope of ~ 3.5 (Lü et al. 2017). This ‘late plateau’³ is not expected within the standard afterglow models, and additional energy injection is needed. If we assume the sharp decay following the internal plateau is due to the collapse of a supra-massive magnetar, then the energy injection required by the late plateau of GRB 160821B can only be provided by the new-born BH. In this case, the late X-ray plateau suggests a possible signature of a new-born BH from the collapse of a supra-massive magnetar.

Motivated by the special X-ray light curve of GRB

160821B, in this paper, we attempt to answer the following questions: What are the possible mechanisms for the long-lasting X-ray emission after the collapse of a supra-massive magnetar to a BH? What types of X-ray signatures can be expected from the new-born BH? Besides GRB 160821B, are there other short GRBs with an internal plateau showing these X-ray signatures? Recently, Chen et al. (2017) found that the X-ray bump following the internal plateau of long GRB 070110 is a possible signature of a new-born BH from the collapse of a supra-massive magnetar and interpreted the X-ray bump as the result of a fall-back accretion onto the BH. Their work further encourages us to explore the possible X-ray signatures of the new-born BH in the case of NS-NS mergers, and to search for these signatures in the sample of short GRBs that show an internal plateau.

This paper is organized as follows. In Section 2, we give a general picture of the spin-down of a supra-massive magnetar and the fall-back accretion onto the new-born BH in the case of NS-NS mergers. In particular, we predict the possible X-ray signatures of the new-born BH that could be observed in the afterglows of short GRBs. We then search for the candidates that might show the BH signatures in their X-ray light curves using the sample of short GRBs with an internal plateau and compare our model with observations in Section 3. Finally, we briefly summarize our results and discuss the implications in Section 4. Throughout the paper, we use the standard notation $Q_x = Q/10^x$ with Q being a generic quantity in cgs units, and a concordance cosmology with parameters $H_0 = 71 \text{ km s}^{-1} \text{ Mpc}^{-1}$, $\Omega_M = 0.30$, and $\Omega_\Lambda = 0.70$ is adopted (Jarosik et al. 2011). All the errors are quoted at the 1σ confidence level.

2 MODEL

Our model assumes that the product of the NS-NS merger is a supra-massive magnetar, as it spins down, it collapses to a BH when the centrifugal force is insufficient to support the mass. We interpret the internal plateau of short GRBs as the magnetic dipole emission from the magnetar and attribute the late X-ray emission (for GRB 160821B, it is a late plateau plus a steep decay) to a process of fall-back accretion onto the new-born BH. Our main work in this section is to explore the possible long-lasting X-ray signatures of the new-born BH.

2.1 Dipole Spin-Down of a Supra-massive Magnetar

Numerical simulations show that NS-NS mergers could eject a fraction of the materials, forming a mildly anisotropic outflow (the so-called ‘dynamical ejecta’) with a typical mass of $\sim 10^{-4} - 10^{-2} M_\odot$ and a typical velocity of $\sim 0.1 - 0.3 c$ (e.g., Rezzolla et al. 2011; Hotokezaka et al. 2013; Rosswog, Piran & Nakar 2013; Ciolfi et al. 2017). The dynamical ejecta are followed by a slower outflow of material that does not exceed the escape velocity and might fall back onto the remnant at later times. The amount of fall-back matter is comparable to or larger than that of the escaping ejecta (e.g., Rosswog 2007; Hotokezaka et al. 2013; Ciolfi et al. 2017), and this material is prone to return within

² The convention $F_\nu \propto \nu^{-\beta} t^{-\alpha}$ is adopted throughout the paper, where β is the spectral index and α is the temporal decay index.

³ Hereafter we use the term ‘late plateau’ to denote the long-lasting plateau following the internal plateau and the sharp decay phase.

a few seconds and create a new ring at a radius of around 300–500 km (Lee, Ramirez-Ruiz & López-Cámara 2009).

In the case of the millisecond magnetar engine, the magnetar would interact with the infalling material via accretion and propeller processes (e.g., Piro & Ott 2011). These processes affect the dipole spin-down and may produce intense electromagnetic emission (e.g., Gompertz, O’Brien & Wynn 2014; Gibson et al. 2017). However, considering the small fall-back mass combined with accretion disc heating effects, the influence on the spin period is not important (Rowlinson et al. 2013; Ravi & Lasky 2014). In addition, the post-merger magnetar may undergo important gravitational wave (GW) radiation (e.g., Zhang & Mészáros 2001; Corsi & Mészáros 2009; Fan, Wu & Wei 2013; Dall’Osso et al. 2015; Doneva, Kokkotas & Pnigouras 2015; Lasky & Glampedakis 2016; Gao, Cao & Zhang 2017), during which a significant spin energy is taken away by GWs. This affects the magnetar spin-down and the collapse time (Gao, Zhang & Lü 2016). Alternatively, the GW effect could be effectively taken into account by choosing a relatively large initial spin period within the dipole spin-down framework as a first approximation (e.g., Rowlinson et al. 2013; Lü et al. 2015). In fact, we will see in this subsection that one can give only the upper limits of the magnetar parameters (period and magnetic field strength) by modeling the observed internal plateaus, considering the above effects would complicate our calculations and give no meaningful results. In this work, we thus do not consider the effects of the magnetar accretion and propeller and GW losses on its spin evolution, and use the simple dipole spin-down model (Zhang & Mészáros 2001).

The characteristic spin-down luminosity L_0 and the characteristic spin-down timescale τ are related to the magnetar initial parameters as (Zhang & Mészáros 2001)

$$L_0 = 1.0 \times 10^{49} \text{ erg s}^{-1} \left(B_{p,15}^2 P_{0,-3}^{-4} R_6^6 \right), \quad (1)$$

$$\tau = 2.05 \times 10^3 \text{ s} \left(I_{45} B_{p,15}^{-2} P_{0,-3}^2 R_6^{-6} \right), \quad (2)$$

where I is the moment of inertia, B is the surface magnetic field strength at the poles, P_0 is the initial spin period, and R is the radius of the magnetar.

The isotropically equivalent luminosity of the internal plateau (L_{int}) is related to the spin-down luminosity L_0 as

$$L_{\text{int}} = (\eta_X / f_b) L_0, \quad (3)$$

where η_X is the radiation efficiency, and $f_b = 1 - \cos \theta_j$ is the beaming factor.

The spin-down formula due to dipole radiation is given by

$$P(t) = P_0 \left(1 + \frac{t}{\tau} \right)^{1/2}. \quad (4)$$

A supra-massive magnetar is temporarily supported by rigid rotation, which could enhance the maximum gravitational mass (M_{max}) allowed for NS surviving. For a given EOS, one can write M_{max} as a function of the spin period P (Lyford, Baumgarte & Shapiro 2003),

$$M_{\text{max}} = M_{\text{TOV}} \left(1 + \hat{\alpha} P^{\hat{\beta}} \right), \quad (5)$$

where M_{TOV} is the maximum mass for a non-rotating NS, $\hat{\alpha}$ and $\hat{\beta}$ depend on the EOS.

The supra-massive magnetar collapses when its spin period becomes large enough that $M_{\text{max}}(P) = M_p$, where M_p is the mass of the protomagnetar. Using Equations (4) and (5), one can derive the collapse time t_{col} ⁴ (Lasky et al. 2014; Lü et al. 2015), i.e.,

$$\begin{aligned} t_{\text{col}} &= \frac{3c^3 I}{4\pi^2 B_p^2 R^6} \left[\left(\frac{M_p - M_{\text{TOV}}}{\hat{\alpha} M_{\text{TOV}}} \right)^{2/\hat{\beta}} - P_0^2 \right] \\ &= \frac{\tau}{P_0^2} \left[\left(\frac{M_p - M_{\text{TOV}}}{\hat{\alpha} M_{\text{TOV}}} \right)^{2/\hat{\beta}} - P_0^2 \right]. \end{aligned} \quad (6)$$

The collapse time of the supra-massive magnetar can be generally identified as the plateau break time in the source frame, i.e., $t_{\text{col}} \simeq t_{\text{b,int}}$. Since the post-plateau decay slope is typically steeper than 3, the spin-down timescale should be greater than the break time. We thus take t_{col} as the lower limit of the spin-down timescale. The magnetar parameters P_0 and B_p can be solved from Equations (1) and (2), i.e.,

$$P_{0,-3} = 1.42 \text{ s} \left(I_{45}^{1/2} L_{0,49}^{-1/2} \tau_3^{-1/2} \right), \quad (7)$$

$$B_{p,15} = 2.05 \text{ G} \left(I_{45} R_6^{-3} L_{0,49}^{-1/2} \tau_3^{-1} \right). \quad (8)$$

With the plateau luminosity L_{int} and the break time $t_{\text{b,int}}$, one can derive the upper limits of P_0 and B_p from Equations (3), (7) and (8) when the NS EOS and the value of η_X/f_b are assumed. When a reasonable value of P_0 in the range of $P_{0,\text{min}} \leq P_0 \leq P_{0,\text{max}}$ is adopted⁵, we can derive M_p from Equation (6) based on the data and a given EOS.

The NS EOS is most uncertain. Using the general relativistic hydrostatic equilibrium code RNS (Stergioulas & Friedman 1995), the numerical values for M_{TOV} , R , I and thus $\hat{\alpha}$ and $\hat{\beta}$ for several EOSs have been worked out (Lasky et al. 2014). More EOSs, especially those for quark star, were studied in Li et al. (2016). In this work, we adopt the EOS GM1 ($M_{\text{TOV}} = 2.37 M_{\odot}$, $R = 12.05 \text{ km}$, $I = 3.33 \times 10^{45} \text{ g cm}^{-2}$, $\hat{\alpha} = 1.58 \times 10^{-10} \text{ s}^{-\hat{\beta}}$ and $\hat{\beta} = -2.84$), which is favored by the short GBR data under the assumption that the cosmological NS-NS merger systems have the same mass distribution as the observed Galactic NS-NS population (Lasky et al. 2014; Lü et al. 2015; Gao, Zhang & Lü 2016).

2.2 Fall-Back Accretion onto the New-Born BH

Fall-back accretion onto a central BH and the resulting radiation have been intensively studied in the framework of a prompt BH (e.g., Rosswog 2007; Metzger, Piro & Quataert 2008; Lee, Ramirez-Ruiz & López-Cámara 2009; Rossi & Begelman 2009). After the original accretion discs are consumed on a viscous timescale of $\sim 0.1 \text{ s}$, the BH begins to accrete the fall-back matter, the accretion rate of which follows a single PL, i.e., $\dot{M}_{\text{fb}} \propto t^{-5/3}$ (e.g., Rosswog 2007).

If the BH is produced by the collapse of a supra-massive

⁴ When the GW effect is considered, the expression of t_{col} is different from Equation (6) and has been derived by Gao, Zhang & Lü (2016). We refer the reader to see this paper for details.

⁵ Here $P_{0,\text{min}}$ is the break-up limit and $P_{0,\text{max}}$ is the derived upper limit of the spin period.

magnetar as considered in this work, there is no debris disk left (Margalit, Metzger & Beloborodov 2015). Before the BH forms, the fall-back material has already returned and created a disk at a radius of a few hundred kilometres. The magnetar accretion and propeller processes would inevitably decrease the total fall-back mass left for the BH to accrete. We thus expect a smaller fall-back mass M_{fb} in our magnetar scenario than the results obtained from the numerical simulations (e.g., Rosswog 2007; Hotokezaka et al. 2013; Ciolfi et al. 2017).

Another issue to be specified is the mass accretion rate (\dot{M}) of the new-born BH. The relation between \dot{M} and \dot{M}_{fb} is uncertain, but it is plausible to assume that \dot{M} is a fraction of \dot{M}_{fb} ⁶ (e.g., Tchekhovskoy et al. 2014; Kisaka & Ioka 2015), i.e.,

$$\dot{M} = f_{\text{acc}} \dot{M}_{\text{fb}} = \dot{M}_i \left(\frac{\tilde{t}}{\tilde{t}_{\text{PL}}} \right)^{-5/3}, \quad (\tilde{t} > \tilde{t}_{\text{PL}}), \quad (9)$$

where $0 < f_{\text{acc}} \leq 1$ is a proportionality constant, $\dot{M}_i = 2f_{\text{acc}}M_{\text{fb}}/(3\tilde{t}_{\text{PL}})$ is the initial mass accretion rate, \tilde{t} is the time since the BH accretion, and \tilde{t}_{PL} denotes the beginning time of such a PL accretion. We use t_0 to denote the beginning time of the BH accretion and approximately set it to be the collapse time, i.e., $t_0 \simeq t_{\text{col}}$. The value of \tilde{t}_{PL} is uncertain, but a conservative estimation of $\tilde{t}_{\text{PL}} \sim 1$ s seems to be reasonable (e.g., Rosswog 2007; Metzger, Piro & Quataert 2008; Lee, Ramirez-Ruiz & López-Cámara 2009; Fernández et al. 2015).

Energy extraction from the BH-accretion disk system can be via neutrino-antineutrino annihilation (Popham, Woosley & Fryer 1999; Narayan, Piran & Kumar 2001; Di Matteo, Perna & Narayan 2002; Gu, Liu & Lu 2006; Chen & Beloborodov 2007; Janiuk et al. 2007; Lei et al. 2009; Liu et al. 2015; Xie, Lei & Wang 2016), or Blandford-Znajek mechanism (BZ, hereafter; Blandford & Znajek 1977; Lee, Wijers & Brown 2000; Li 2000; Lei, Wang & Ma 2005; Lei, Zhang & Liang 2013). In the case of fall-back accretion, the neutrino-antineutrino annihilation becomes inefficient quickly (> 0.1 s; Rossi & Begelman 2009; Metzger, Piro & Quataert 2008) and cannot explain the late X-ray emission observed in short GRBs with an internal plateau (e.g., the late plateau of GRB 160821B). The BZ process remains a possible mechanism that power the long-lasting X-ray emission.

The BZ process extracts the BH rotational energy via the large-scale poloidal magnetic field that is supported by the surrounding torus (Blandford & Znajek 1977; Lee, Wijers & Brown 2000). For a Kerr BH with mass M_{\bullet} ($\equiv m_{\bullet}M_{\odot}$) and angular momentum J_{\bullet} , the BZ power can be estimated as (Lee, Wijers & Brown 2000; Li 2000; Wang, Xiao & Lei 2002; McKinney 2005; Lei & Zhang 2011; Lei, Zhang & Liang 2013)

$$L_{\text{BZ}} = 1.7 \times 10^{50} \text{ erg s}^{-1} a_{\bullet}^2 m_{\bullet}^2 B_{\bullet,15}^2 F(a_{\bullet}), \quad (10)$$

⁶ For the mass accretion rate of a BH, Metzger, Piro & Quataert (2008) found $\dot{M} \propto t^{-4/3}$ for an advection-dominated disk, while the numerical simulation results of Fernández et al. (2015) showed $\dot{M} \propto t^{-2.2}$ ($1 \text{ s} \lesssim t \lesssim 10 \text{ s}$) when the display between the disk winds and the dynamical ejecta is considered. However, it is unclear whether these scale laws apply to large time scales (e.g., $t \gtrsim 100 \text{ s}$).

where $a_{\bullet} = J_{\bullet}c/(GM_{\bullet}^2)$ is the dimensionless spin parameter of the BH, B_{\bullet} is the magnetic field strength threading the BH horizon. The spin-dependent function $F(a_{\bullet})$ can be approximated as (Lee, Wijers & Brown 2000; Wang, Xiao & Lei 2002)

$$F(a_{\bullet}) = \left[\left(1 + q^2 \right) / q^2 \right] [(q + 1/q) \arctan q - 1], \quad (11)$$

where $q = a_{\bullet}/(1 + \sqrt{1 - a_{\bullet}^2})$, and $2/3 \leq F(a_{\bullet}) \leq \pi - 2$ for $0 \leq a_{\bullet} \leq 1$. Tchekhovskoy, Narayan, & McKinney (2010) investigated this function numerically and gave an analytical fit to the numerical model. Their obtained function is similar to Equation (11) at most a_{\bullet} values and only slightly deviates from it as a_{\bullet} approaches 1. We thus use Equation (11) as a reasonable approximation.

A major uncertainty in estimating the BZ power is the strength of magnetic fields (Kumar & Zhang 2015). Because of the freedom in B_{\bullet} , for a fixed value of BH spin a_{\bullet} and mass accretion rate \dot{M} , we expect a range of BZ powers from zero (no jet) up to a maximum value (Tchekhovskoy et al. 2015). By performing advanced numerical simulations, Tchekhovskoy, Narayan & McKinney (2011) demonstrated that accretion disks can accumulate large-scale magnetic flux ($\Phi_{\bullet} \sim \pi r_{\bullet}^2 B_{\bullet}$) on the BH, until the magnetic flux becomes so strong that it obstructs gas infall and leads to a magnetically-arrested disk (MAD; Bisnovatyi-Kogan & Ruzmaikin 1974, 1976; Igumenshchev, Narayan & Abramowicz 2003; Narayan, Igumenshchev & Abramowicz 2003). Since the BH magnetic flux is maximum in the MAD state, MADs achieve the maximum possible efficiency of jet production (Tchekhovskoy, Narayan & McKinney 2011). These results were later used in the areas of active galactic nuclei, tidal disruptions events, and GRBs (e.g., Tchekhovskoy et al. 2014; Zamaninasab et al. 2014; Kisaka & Ioka 2015; Tchekhovskoy & Giannios 2015).

The MAD state happens at a critical mass accretion rate that can be estimated by assuming the magnetic pressure (P_{mag}) and the disk gas pressure (P_{gas}) balance at the BH horizon (e.g., Narayan, Igumenshchev & Abramowicz 2003; Kisaka & Ioka 2015; Tchekhovskoy et al. 2015), i.e.,

$$\frac{B_{\bullet}^2}{8\pi} = \frac{GM_{\bullet}\dot{M}}{2\pi r^3 v_r} \Big|_{r=r_{\bullet}}, \quad (12)$$

where G is the gravitational constant, \dot{M} is the mass accretion rate of the BH, $r_{\bullet} = (1 + \sqrt{1 - a_{\bullet}^2})r_g \equiv \chi(a_{\bullet})r_g$ is the radius of the BH horizon, and $r_g = GM_{\bullet}/c^2$; $v_r = \varepsilon v_{\text{ff}}$ is the radial velocity of the infalling gas outside the horizon, where $v_{\text{ff}} = \sqrt{GM_{\bullet}/r}$ is the free-fall velocity. Since the accretion disk gas diffuses towards the BH via magnetic reconnection and interchanges, the velocity is much less than the free-fall velocity. It is reasonable to adopt $\varepsilon = 10^{-2}$ (Narayan, Igumenshchev & Abramowicz 2003; Kisaka & Ioka 2015), which is supported by the observations and numerical simulations of the relativistic jets (e.g., Tchekhovskoy, Narayan & McKinney 2011; Zamaninasab et al. 2014). From Equation (12), one can derive

$$\begin{aligned} \dot{M}_{\text{MAD}} &= 8.2 \times 10^{-12} M_{\odot} \text{ s}^{-1} \chi^{5/2} \left(\frac{\varepsilon}{10^{-2}} \right) \\ &\times \left(\frac{B_{\bullet}}{10^{12} \text{ G}} \right)^2 \left(\frac{m_{\bullet}}{3} \right)^2. \end{aligned} \quad (13)$$

The initial accretion rate $\dot{M}_i = 2f_{\text{acc}}M_{\text{fb}}/(3\tilde{t}_{\text{PL}}) \sim 10^{-5} - 10^{-3}M_{\odot} \text{ s}^{-1}$ if we adopt $M_{\text{fb}} \sim 10^{-4} - 10^{-2}M_{\odot}$, $f_{\text{acc}} = 0.5$ and $\tilde{t}_{\text{PL}} = 1$ s. As long as B_{\bullet} is not much larger than 10^{14} G, we have $\dot{M}_i \gg \dot{M}_{\text{MAD}}$. According to Equation (12), this is equivalent to say $P_{\text{gas}} \gg P_{\text{mag}}$. In this case, the gas accreted onto the new-born BH is more than sufficient to confine the magnetic flux within the BH vicinity. As long as $\dot{M} \geq \dot{M}_{\text{MAD}}$, the BZ power is determined by the magnetic flux Φ_{\bullet} and not by mass accretion rate. During this phase (‘pre-MAD’ hereafter), the BZ power $L_{\text{BZ}} \propto a_{\bullet}^2 m_{\bullet}^2 B_{\bullet}^2 \propto a_{\bullet}^2 m_{\bullet}^{-2} \Phi_{\bullet}^2$ is roughly a constant (Tchekhovskoy & Giannios 2015; Kisaka & Ioka 2015). As \dot{M} decreases and eventually drops below \dot{M}_{MAD} , we have $P_{\text{gas}} < P_{\text{mag}}$, then the magnetic flux becomes dynamically important, and parts of the flux diffuse out. The remaining magnetic flux obstructs gas infall and leads to a MAD (Tchekhovskoy & Giannios 2015). In the MAD regime, the magnetic field (and thus the magnetic flux) is determined by the instantaneous \dot{M} via Equation (13), i.e., $B_{\bullet} \propto \dot{M}^{1/2}$ (Tchekhovskoy & Giannios 2015). Thus, the BZ power $L_{\text{BZ}} \propto B_{\bullet}^2 \propto \dot{M}$ is a function of mass accretion rate.

Taking into account the X-ray radiation efficiency $\eta_{\bullet, X}$ and the beaming factor $f_{\bullet, b}$, the observed isotropic X-ray luminosity can be written as

$$L_{X, \text{iso}} = (\eta_{\bullet, X}/f_{\bullet, b})L_{\text{BZ}}. \quad (14)$$

We assume that the MAD is achieved at $\tilde{t} = \tilde{t}_{\text{MAD}}$. In this time coordinate system, the light curve shows a plateau in the pre-MAD regime ($\tilde{t} \leq \tilde{t}_{\text{MAD}}$), followed by a single PL with the decay slope consistent with \dot{M} in the MAD regime ($\tilde{t} > \tilde{t}_{\text{MAD}}$).

The plateau luminosity L_{preMAD} can be obtained straightforwardly from Equations (10) and (14),

$$L_{\text{preMAD}} = 1.5 \times 10^{43} \text{ erg s}^{-1} \left(\frac{\eta_{\bullet, X}/f_{\bullet, b}}{1} \right) \left(\frac{a_{\bullet}}{0.1} \right)^2 \times F(a_{\bullet}) \left(\frac{B_{\bullet, \text{MAD}}}{10^{12} \text{ G}} \right)^2 \left(\frac{m_{\bullet}}{3} \right)^2, \quad (15)$$

where $B_{\bullet, \text{MAD}}$ is the critical magnetic field strength that is related to \dot{M}_{MAD} by Equation (13). It is also the magnetic field strength in the pre-MAD regime and can be determined by observations. The duration of the pre-MAD state and thus the break time of the X-ray plateau can be derived from $\dot{M}(\tilde{t}_{\text{MAD}}) = \dot{M}_{\text{MAD}}$. Using Equations (9) and (13), we obtain

$$\begin{aligned} \tilde{t}_{\text{MAD}} &= 3.7 \times 10^4 \text{ s } \chi^{-3/2} \left(\frac{\varepsilon}{10^{-2}} \right)^{-3/5} \left(\frac{f_{\text{acc}}}{0.5} \right)^{3/5} \\ &\times \left(\frac{\tilde{t}_{\text{PL}}}{1 \text{ s}} \right)^{2/5} \left(\frac{m_{\bullet}}{3} \right)^{-6/5} \\ &\times \left(\frac{M_{\text{fb}}}{10^{-3} M_{\odot}} \right)^{3/5} \times \left(\frac{B_{\bullet, \text{MAD}}}{10^{12} \text{ G}} \right)^{-6/5}. \end{aligned} \quad (16)$$

During the MAD phase, the X-ray luminosity $L_{X, \text{iso}} \propto \dot{M} \propto \tilde{t}^{-5/3}$. Then we can model the luminosity evolution as

$$\begin{aligned} L_{X, \text{iso}}(\tilde{t}) &= L_{\text{preMAD}} \left(1 + \frac{\tilde{t}}{\tilde{t}_{\text{MAD}}} \right)^{-5/3}, \\ &\approx \begin{cases} L_{\text{preMAD}}, & 0 < \tilde{t} \ll \tilde{t}_{\text{MAD}}, \\ L_{\text{preMAD}} \left(\frac{\tilde{t}}{\tilde{t}_{\text{MAD}}} \right)^{-5/3}, & \tilde{t} \gg \tilde{t}_{\text{MAD}}. \end{cases} \end{aligned} \quad (17)$$

As seen from Equation (17), in the \tilde{t} coordinate system, the

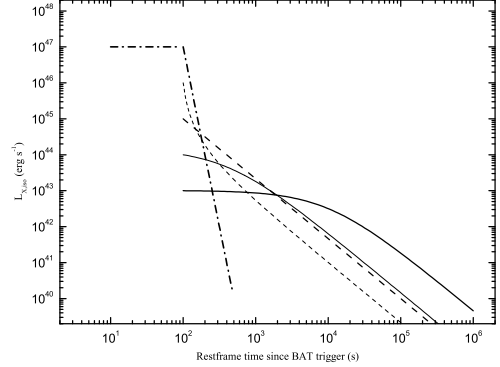


Figure 1. Theoretical X-ray light curves produced by the dipole spin-down of a supra-massive magnetar and the BZ process of the new-born BH. The magnetar radiation component is shown with dotted dash lines. The following magnetar parameters are adopted: the spin-down luminosity $L_0 = 10^{47} \text{ erg s}^{-1}$, the collapse time $t_{\text{col}} = 100$ s and the decay slope following the collapse $\alpha = 10$. The BH radiation component is drawn according to Equation (20). A series of values of L_{preMAD} and \tilde{t}_{MAD} are used in order to show different luminosity evolutions. The adopted parameters and the resulting light curves are: $L_{\text{preMAD}} = 10^{43} \text{ erg s}^{-1}$, $\tilde{t}_{\text{MAD}} = 10^4$ s (thick solid line); $L_{\text{preMAD}} = 10^{44} \text{ erg s}^{-1}$, $\tilde{t}_{\text{MAD}} = 500$ s (thin solid line); $L_{\text{preMAD}} = 10^{45} \text{ erg s}^{-1}$, $\tilde{t}_{\text{MAD}} = 100$ s (thick dashed line); $L_{\text{preMAD}} = 10^{46} \text{ erg s}^{-1}$ and $\tilde{t}_{\text{MAD}} = 10$ s (thin dashed line).

predicted X-ray luminosity exhibits an initial plateau before \tilde{t}_{MAD} , then decays as $\tilde{t}^{-5/3}$.

According to Equations (15) and (16), when the values of a_{\bullet} , m_{\bullet} , $B_{\bullet, \text{MAD}}$ and M_{fb} are given, we can model the observed X-ray light curve straightforwardly. Conversely, these parameters can be obtained by modeling the afterglow data. Among of them, $B_{\bullet, \text{MAD}}$ and M_{fb} can be derived as follows.

From Equation (15), the magnetic field strength $B_{\bullet, \text{MAD}}$ is given by

$$\begin{aligned} B_{\bullet, \text{MAD}} &= 7.8 \times 10^{11} \text{ G} \left(\frac{a_{\bullet}}{0.1} \right)^{-1} \left(\frac{m_{\bullet}}{3} \right)^{-1} F^{-1/2}(a_{\bullet}) \\ &\times \left(\frac{\eta_{\bullet, X}/f_{\bullet, b}}{1} \right)^{-1/2} \left(\frac{L_{\text{preMAD}}}{10^{43} \text{ erg s}^{-1}} \right)^{1/2}. \end{aligned} \quad (18)$$

Then the total fall-back mass M_{fb} can be obtained from Equations (16) and (18),

$$\begin{aligned} M_{\text{fb}} &= 6.7 \times 10^{-5} M_{\odot} \left(\frac{f_{\text{acc}}}{0.5} \right)^{-1} \left(\frac{\eta_{\bullet, X}/f_{\bullet, b}}{1} \right)^{-1} \\ &\times \left(\frac{\varepsilon}{10^{-2}} \right) \left(\frac{a_{\bullet}}{0.1} \right)^{-2} \chi^{5/2} F^{-1}(a_{\bullet}) \\ &\times \left(\frac{\tilde{t}_{\text{PL}}}{1 \text{ s}} \right)^{-2/3} \left(\frac{L_{\text{preMAD}}}{10^{43} \text{ erg s}^{-1}} \right) \left(\frac{\tilde{t}_{\text{MAD}}}{10^4 \text{ s}} \right)^{5/3}. \end{aligned} \quad (19)$$

We note that $M_{\text{fb}} \propto \tilde{t}_{\text{PL}}^{-2/3}$ is not strongly dependent on \tilde{t}_{PL} , so the value of \tilde{t}_{PL} adopted in our modeling will not have a significant influence on the derived M_{fb} .

To compare with observations, we need to transform the coordinate system from \tilde{t} to t by doing $\tilde{t} \rightarrow t - t_{\text{col}}$. Then the X-ray luminosity can be written as

$$L_{X, \text{iso}}(t) = L_{\text{preMAD}} \left(1 + \frac{t - t_{\text{col}}}{\tilde{t}_{\text{MAD}}} \right)^{-5/3}, \quad t > t_{\text{col}}. \quad (20)$$

A plateau-like feature can be found only if $\tilde{t}_{\text{MAD}} \gg t_{\text{col}}$. To show this clearly, we draw the theoretical light curves according to Equation (20), with a series of values of L_{preMAD} from 10^{43} to 10^{46} erg s $^{-1}$ and the corresponding \tilde{t}_{MAD} from 10^4 to 10 s. As seen from Figure 1, the light curve pattern strongly depends on the value of \tilde{t}_{MAD} . When $\tilde{t}_{\text{MAD}} \gg t_{\text{col}}$, the light curve shows a long-lasting plateau (e.g., the thick solid line); it reveals a gradual transition from a plateau to a single PL as \tilde{t}_{MAD} approaches $\sim t_{\text{col}}$ (e.g., from the thin solid line to the thick dashed line); as \tilde{t}_{MAD} further decreases, the light curve shows an initial steep decay followed by a smooth transition to a single PL with slope of 5/3 (e.g., the thin dashed line). We note that the light curve pattern is very sensitive to the values of L_{preMAD} and \tilde{t}_{MAD} . Thus, these parameters can, in principle, be obtained by modeling the afterglow data with Equation (20).

The physics is easy to understand. With Equations (10), (13) and $\dot{M}_{\text{MAD}} = \dot{M}_i (\tilde{t}_{\text{MAD}}/\tilde{t}_{\text{PL}})^{-5/3}$, we have $\tilde{t}_{\text{MAD}} \propto B_{\bullet, \text{MAD}}^{-6/5} \dot{M}_i^{3/5}$ and $L_{\text{preMAD}} \propto B_{\bullet, \text{MAD}}^2$. For the same \dot{M}_i , higher $B_{\bullet, \text{MAD}}$ corresponds to smaller \tilde{t}_{MAD} and higher L_{preMAD} , and vice versa. Therefore, if the pre-MAD state can sustain a high magnetic field strength, say, $B_{\bullet, \text{MAD}} \sim 10^{14}$ G, it would result in a small $\tilde{t}_{\text{MAD}} \sim t_{\text{col}}$ according to Equation (16) for typical parameters. Though the light curve shows a short plateau in the \tilde{t} coordinate system, this plateau cannot be seen after the time transformation. In this case, the light curve is roughly a single PL. Conversely, if the pre-MAD state has a weak magnetic field, say, $B_{\bullet, \text{MAD}} \sim 10^{12}$ G, then the resulting \tilde{t}_{MAD} is much longer than t_{col} . This produces a long-lasting plateau in the light curve, followed by a temporal decline with slope of 5/3. Therefore, the light curve patterns are mostly determined by the pre-MAD magnetic field strength. They are, however, also weakly affected by the initial accretion rate or the total fall-back mass via $\tilde{t}_{\text{MAD}} \propto B_{\bullet, \text{MAD}}^{-6/5} \dot{M}_i^{3/5} \propto B_{\bullet, \text{MAD}}^{-6/5} \dot{M}_{\text{fb}}^{3/5}$.

It should be noted that, when the pre-MAD phase lasts a very long time, say, $\tilde{t}_{\text{MAD}} \sim 10^4$ s, the critical accretion rate is $\dot{M}_{\text{MAD}} \sim 10^{-11} M_{\odot} \text{ s}^{-1}$ according to Equation (13). Whether such a low accretion rate can sustain the MAD state is questionable. [Kisaka & Ioka \(2015\)](#) considered an extreme case by assuming that the fall-back matter is too small to support the magnetic flux at the end of the pre-MAD regime. In this case, the MAD state cannot be achieved, and the magnetic field lines escape rapidly from the BH. They thus used a very large post-plateau decay slope of 40/9⁷. For a short pre-MAD, however, \dot{M}_{MAD} is relatively high and we assume the MAD state can be achieved⁸. Therefore, we use the decay index of $\alpha_1 = 5/3$ to 40/9 in Equation (20) only for the light curve that shows a long-lasting plateau. For other cases, we use $\alpha_{\text{II}} = 5/3$ that is consistent with the decay of \dot{M} in the MAD state.

⁷ This value was derived based on the flux conversation. The balance between the magnetic pressure and the gas pressure gives the magnetospheric radius r_m . As \dot{M} decreases, r_m expands as $r_m \propto \dot{M}^{10/9}$. The magnetic flux $\Phi_{\bullet} \propto r_m^{-2}$, then $L_X \propto L_{\text{BZ}} \propto \Phi_{\bullet}^2 \propto \dot{M}^{-40/9}$ ([Kisaka & Ioka 2015](#)).

⁸ In principle, we should expect a change of slope from 5/3 to 40/9 at late times when the MAD state cannot be sustained. However, since it is difficult to predict when such a change occurs, we do not consider this extreme case and simply assume that the MAD state lasts long enough.

In summary, when the entire physical processes from a supra-massive magnetar to the new-born BH are considered, our model predicts two types of typical X-ray light curves (see Figure 1 for the detailed evolutions however):

- Type I: an internal plateau plus a sharp drop with slope of $\alpha > 3$, followed by a long-lasting plateau plus a steep decay with slope of $\alpha_1 = 5/3$ to 40/9. The luminosity of the late plateau is roughly constant and the duration is $\sim 10^4$ s for typical parameters (see Equation (16));
- Type II: an internal plateau plus a sharp drop, followed by a PL decay with slope of $\alpha_{\text{II}} = 5/3$.

We emphasize that type I and II light curves are intrinsically produced by the same physical process. It is the ‘zero point effect’ that makes their light curves look different. In the \tilde{t} coordinate system, a plateau-like feature with duration $\sim \tilde{t}_{\text{MAD}}$ always exists. When transforming to the t coordinate system (the zero time is usually set to the trigger time), the existence of plateau depends on the relation between the values of t_0 ($= t_{\text{col}}$) and \tilde{t}_{MAD} . Type I corresponds to $\tilde{t}_{\text{MAD}} \gg t_0$ while type II requires that \tilde{t}_{MAD} is smaller or comparable with t_0 .

3 OBSERVATIONAL SUPPORT

In this section, we first search for the theoretically predicted X-ray light curves from a sample of short GRBs with an internal plateau, then compare our model with the data.

3.1 Candidate Search

For a complete search of the candidates, we set up three criteria for sample selection: (1) We focus on short GRBs with an internal plateau that has a post-plateau decay slope of $\alpha > 3$. (2) We focus on bursts with high-quality post-plateau data, in particular, we require the late X-ray data clearly show a feature deviating from the sharp decay phase, and span a wide range of time to show a clear temporal evolution. (3) We further require the data to resemble our theoretically predicted light curves, that is, the late X-ray data should show a plateau with slope of ~ 0 or a single PL decay with slope of $\sim 5/3$.

The properties of X-ray afterglow of short GRBs with an internal plateau have been systematically studied by [Rowlinson et al. \(2013\)](#)⁹ and [Lü et al. \(2015\)](#). Using their samples, we find 11 firm candidates that clearly show an internal plateau. These candidates are the same as those bursts that were marked with ‘unstable’ magnetars in Table 6 of [Rowlinson et al. \(2013\)](#). This sample is further reduced based on criterion (2) and we find only two bursts that satisfy this requirement. Together with GRB 160821B, the sample thus includes three bursts, which are GRB 070724A, GRB 101219A and GRB 160821B. As stated in Section 1, GRB 160821B shows a late plateau with slope of ~ 0.45 and is marginally consistent with our type I light curve. The

⁹ The definition of ‘internal plateau’ used in our paper is actually consistent with the description in [Rowlinson et al. \(2013\)](#) that the X-ray plateau followed by a sharp drop which may suggest a magnetar collapsing to a BH.

late X-ray data of GRB 101219A exhibit a single PL decay with slope of ~ 1.9 (Evans et al. 2009), resembling our type II light curve. The light curve of GRB 070724A, however, is quite different. The late X-ray data show a shallow decay with slope of $0.65^{+0.10}_{-0.12}$, followed by a steep decay with slope of 3^{+2}_{-1} (Ziaeeepour et al. 2007). The spectral index during this phase is $\beta_X \approx 0.5$ (Kocevski et al. 2010). The slope of the shallow decay phase is consistent with the prediction of the standard afterglow model when the X-ray frequency ν_X is in the energy range of $\nu_m < \nu_X < \nu_c$, where ν_m and ν_c are the typical synchrotron frequency and the cooling frequency of electrons, respectively (Sari, Piran & Narayan 1998). This is also supported by the near-infrared (NIR) and optical afterglow observations (Berger et al. 2009). We thus do not consider this burst in the following analysis. Therefore, the final candidates include two bursts: GRB 101219A and GRB 160821B.

The *Swift* BAT and X-ray Telescope (XRT; Burrows et al. 2005) data are downloaded from the *Swift* website¹⁰. The 0.3–10 keV unabsorbed X-ray flux was reduced by an automatic analysis procedure, and the BAT (15–150 keV) data were extrapolated to the XRT band (0.3–10 keV) (Evans et al. 2007, 2009). Fortunately, both bursts have redshift measurements, we thus transform the flux data to the luminosity light curve in the observed 0.3–10 keV energy band (see Figures 2 and 3).

3.2 Case Study

3.2.1 GRB 160821B

GRB 160821B triggered the *Swift*/BAT at 22:29:13 UT on 2016 August 21 (Siegel et al. 2016). It was also detected by the *Fermi* Gamma-ray Burst Monitor (GBM) almost simultaneously (Stanbro & Meegan 2016). The BAT light curve shows a single short peak with duration $T_{90} = 0.48 \pm 0.07$ s (Palmer et al. 2016). The time-integrated BAT+GBM spectrum can be jointly fit by a single PL with photon index $\Gamma_\gamma = 1.88 \pm 0.12$. The total fluence in the 8–1000 keV range is $(2.52 \pm 0.19) \times 10^{-6}$ erg cm⁻², with a redshift of $z = 0.16$ (Levan et al. 2016), this corresponds to an isotropically equivalent energy $E_{\gamma, \text{iso}} = (2.1 \pm 0.2) \times 10^{50}$ erg (Lü et al. 2017).

The XRT began observing the field 66 s after the BAT trigger (Siegel et al. 2016). The X-ray spectrum in the 0.3–10 keV energy band is best fit by an absorbed PL with photon index $\Gamma_X = 1.95^{+0.21}_{-0.08}$ and column density $N_H = (7.5 \pm 2.1) \times 10^{20}$ cm⁻² (Lü et al. 2017). The light curve shows an initial plateau lasting for ~ 180 s then drops smoothly along with the Γ_X evolution from ~ 2 to ~ 3 . After about 1000 s, the light curve shows a late plateau followed by a steep decay and the photon index during this phase is ~ 3 (Lü et al. 2017). The Ultra-Violet Optical Telescope (UVOT; Roming et al. 2005) began settled observations of the field of GRB 160821B 76 s after the BAT trigger, but no optical afterglow consistent with the XRT position (Evans et al. 2016) was detected. Only preliminary 3σ upper limits are obtained by using the UVOT photometric system for the first finding chart exposure (Breeveld & Siegel 2016).

In addition, possible macronova emission was reported in this burst (Troja et al. 2016; Kasliwal et al. 2017).

With the X-ray data of GRB 160821B and our model described in Section 2, we can now constrain the model parameters ($P_0, B_p, M_p, a_\bullet, B_{\bullet, \text{MAD}}, M_{\text{fb}}$) and then compare our model with the data. For the magnetar parameters, we use the data of the internal plateau: $L_{\text{int}} \simeq 1.2 \times 10^{47}$ erg s⁻¹ and $t_{\text{b, int}} \simeq 180/(1+z)$ s = 155 s (Lü et al. 2017). By assuming $\eta_X/f_b = 1$ ¹¹ and the EOS GM1, we obtain the upper limits of P_0 and B_p using Equations (3), (7) and (8), i.e., $P_0 \lesssim 60$ ms, $B_p \lesssim 2.3 \times 10^{17}$ G. Within the magnetar model, Rowlinson et al. (2013) and Lü et al. (2015) investigated a dozen of short GRBs with an internal plateau, and found that most bursts have P_0 and B_p values in the ranges of 1–10 ms and 10^{15} – 10^{16} G, respectively (see also Gao, Zhang & Lü 2016). Without loss of generality, we adopt $P_0 = 4$ ms. As stated in Section 2, this relatively large P_0 is taken by equivalently considering angular momentum loss via strong GW radiation. Then we have $B_p = 1.0 \times 10^{15}$ G and $\tau = 3.6 \times 10^4$ s according to Equations (1) and (2). Using Equation (6), we obtain the mass of the supra-massive magnetar $M_p \simeq M_{\text{TOV}} = 2.37M_\odot$.

With the above magnetar parameters, we get the mass and spin of the new-born BH, i.e., $M_\bullet \simeq 2.37M_\odot$ and $a_\bullet \simeq 0.1$ (by using $J_\bullet = 2\pi I/P_0$). For other parameters, we use the data of the late plateau. Since the theoretically predicted post-plateau decay slope is uncertain, ranging from 5/3 to 40/9, we consider two cases: (a) For $\alpha_1 = 5/3$, we adopt the plateau luminosity $L_{\text{preMAD}} = 8 \times 10^{43}$ erg s⁻¹ and the plateau duration $\tilde{t}_{\text{MAD}} = 3 \times 10^4/(1+z)$ s $\simeq 2.6 \times 10^4$ s. By assuming $\eta_{\bullet, X}/f_{\bullet, b} = 1$ and $f_{\text{acc}} = 0.5$, we obtain the magnetic field strength $B_{\bullet, \text{MAD}} \simeq 3.1 \times 10^{12}$ G and the total fall-back mass $M_{\text{fb}} \simeq 0.02M_\odot$ from Equations (18) and (19). We note that the value of M_{fb} is consistent with the obtained ejecta mass from numerical simulations (e.g., Hotokezaka et al. 2013; Ciolfi et al. 2017). (b) For $\alpha_1 = 40/9$, we use the same L_{preMAD} , $\eta_{\bullet, X}/f_{\bullet, b}$ and f_{acc} as case (a), except for $\tilde{t}_{\text{MAD}} = 8 \times 10^4$ s. This different choice of \tilde{t}_{MAD} only affects the obtained value of M_{fb} according to Equation (19), and we get $M_{\text{fb}} \simeq 0.1M_\odot$. This value is also compatible with the maximum fall-back mass obtained from numerical simulations (e.g., Hotokezaka et al. 2013; Ciolfi et al. 2017). We note that the derived M_{fb} has a strong dependence on $\eta_{\bullet, X}/f_b$, a_\bullet and \tilde{t}_{PL} according to Equation (19). Smaller M_{fb} can be obtained if we adopt larger values of these parameters.

To compare our model with the data, we use Equations (1), (3), and (15)–(20). According to the fitting results of Lü et al. (2017), we assume the luminosity declines with a slope of 5 after the collapse, and model the sharp decay phase with $L_{X, \text{iso}} = L_{\text{int}}(t/t_{\text{b, int}})^{-5}$.

Figure 2 compares our theoretical 0.3–10 keV light curve with the XRT data. The blue solid line is for $\alpha_1 = 5/3$, while the black dotted line is for $\alpha_1 = 40/9$. For clarity, the latter exhibits only the radiation component produced by the BH.

¹¹ The radiation efficiency η_X and the beaming factor f_b are unknown due to lack of knowledge on the jet production and dissipation process. Without loss of generality, we assume $\eta_X/f_b = 1$, which was used in Rowlinson et al. (2013) and Lü et al. (2015). The statement above also applies to the new-born BH. We thus adopt $\eta_{\bullet, X}/f_{\bullet, b} = 1$ as well in the following estimations.

¹⁰ http://www.swift.ac.uk/burst_analyser/

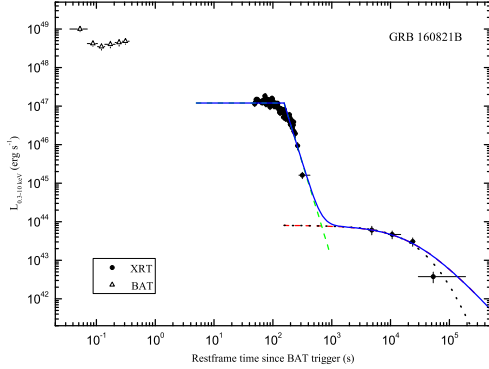


Figure 2. Theoretical light curves as compared with the XRT data of GRB 160821B. The BAT and XRT data are exhibited with empty triangles and filled circles, respectively. The dashed lines are our modeling results for the supra-massive magnetar (green) and the new-born BH (red, for the case of $\alpha_1 = 5/3$), and the blue solid line is the superposition of both components. The adopted parameters are: $P_0 = 4$ ms, $B_p = 1.0 \times 10^{15}$ G, $M_\bullet = M_p = 2.37M_\odot$, $a_\bullet = 0.1$, $B_{\bullet, \text{MAD}} = 3.1 \times 10^{12}$ G, $M_{\text{fb}} = 0.02M_\odot$, $\eta_X/f_b = \eta_{\bullet, X}/f_{\bullet, b} = 1$ and $f_{\text{acc}} = 0.5$. The case for $\alpha_1 = 40/9$ is also shown with black dotted line, but only the BH component is exhibited for clarity. The adopted parameters are the same as given above except for $M_{\text{fb}} = 0.1M_\odot$.

It is shown that our model can describe the luminosity evolution rather well. However, our magnetar model does not explain the smooth transition from the internal plateau to the sharp decay (at around $t_{\text{b, int}}$). Since this transition happens during the magnetar collapse, the data suggest that this process does not result in an abrupt cessation of emission in the X-ray band. Meanwhile, the flux declines along with the spectral evolution (Lü et al. 2017), which may be related to the smooth break in the light curve. The sharp decay phase may be a joint result of the ‘curvature effect’ (e.g., Fenimore, Madras & Nayakshin 1996; Kumar & Panaitescu 2000; Dermer 2004) and the spectral evolution (Zhang et al. 2009).

3.2.2 GRB 101219A

GRB 101219A triggered the *Swift*/BAT at 02:31:29 UT on 2010 December 19 (Gelbord et al. 2010) and was also detected by *Konus-Wind* (Golenetskii et al. 2010). The γ -ray light curve shows a double-peaked structure with $T_{90} = 0.6 \pm 0.2$ s (15–150 keV; Krimm et al. 2010). The time-integrated spectrum is best fit in the 20 keV–10 MeV range by a PL with exponential cutoff model, which gives $E_{\text{pk}} = 490_{-79}^{+103}$ keV and a fluence of $(3.6 \pm 0.5) \times 10^{-6}$ erg cm $^{-2}$ (Golenetskii et al. 2010). With a redshift of $z = 0.718$ (Chornock & Berger 2010), the resulting isotropic γ -ray energy in the observed 20 keV–10 MeV range is $E_{\gamma, \text{iso}} \approx 4.8 \times 10^{51}$ erg (Fong et al. 2013).

The XRT began observing the field 60.5 s after the BAT trigger (Golenetskii et al. 2010). The X-ray spectrum is best fit by an absorbed PL with $\Gamma_X = 1.8 \pm 0.1$ and $N_{\text{H}} = 6.6_{-1.8}^{+2.3} \times 10^{21}$ cm $^{-2}$ (Fong et al. 2013). The light curve exhibits a short plateau before ~ 200 s, then drop sharply,

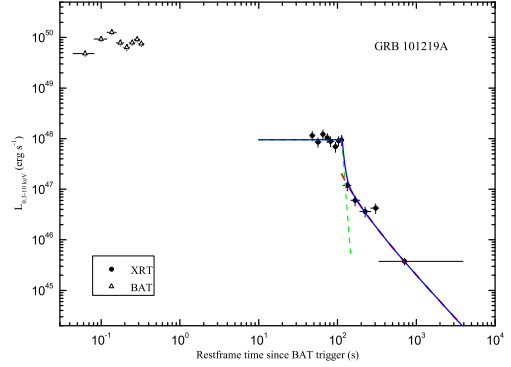


Figure 3. Theoretical light curves as compared with the XRT data of GRB 101219A. The BAT and XRT data are exhibited with empty triangles and filled circles, respectively. The dashed lines are our modeling results for the supra-massive magnetar (green) and the new-born BH (red), and the blue solid line is the superposition of both components. The adopted parameters are: $P_0 = 4$ ms, $B_p = 2.8 \times 10^{15}$ G, $M_\bullet = M_p = 2.37M_\odot$, $a_\bullet = 0.1$, $B_{\bullet, \text{MAD}} = 1.6 \times 10^{14}$ G, $M_{\text{fb}} = 1.9 \times 10^{-3}M_\odot$, $\eta_X/f_b = \eta_{\bullet, X}/f_{\bullet, b} = 1$ and $f_{\text{acc}} = 0.5$.

followed by a single PL decay with slope of 1.91 ± 0.08 (Evans et al. 2009). The *Swift*/UVOT commenced observations 67 s after the BAT trigger. No optical afterglow was detected within the XRT position to a 3σ limit of $\gtrsim 21.4$ mag in the *white* filter (Kuin & Gelbord 2010; Fong et al. 2013). Observations by several ground-based instruments also revealed no optical/NIR counterpart within the XRT error circle, and only 3σ upper limits were given (e.g., Pandey, Zheng & Rujopakarn 2010; Covino & Palazzi 2010; Fong et al. 2013).

The parameters of GRB 101219A can be estimated following the same way as GRB 160821B. For this burst, we also assume $\eta_X/f_b = \eta_{\bullet, X}/f_{\bullet, b} = 1$ and $f_{\text{acc}} = 0.5$. By adopting $L_{\text{int}} = 9.5 \times 10^{47}$ erg s $^{-1}$ and $t_{\text{b, int}} = 113$ s for the luminosity and duration of the internal plateau, we obtain the upper limits of P_0 and B_p : $P_0 \lesssim 25$ ms and $B_p \lesssim 1.1 \times 10^{17}$ G. Here we also adopt $P_0 = 4$ ms, then the corresponding magnetic field strength and spin-down timescale are $B_p \simeq 2.8 \times 10^{15}$ G and $\tau \simeq 4.6 \times 10^3$ s, respectively. Using Equation (6), we obtain the mass of the supra-massive magnetar $M_p \simeq 2.37M_\odot$.

Then the mass and spin of the new-born BH are $M_\bullet \simeq 2.37M_\odot$ and $a_\bullet \simeq 0.1$, respectively. To obtain the values of L_{preMAD} and \tilde{t}_{MAD} , we fit the data with Equation (20) and get $L_{\text{preMAD}} \simeq 2 \times 10^{47}$ erg s $^{-1}$ and $\tilde{t}_{\text{MAD}} \simeq 60$ s. By substituting these values into Equations (18) and (19), we obtain $B_{\bullet, \text{MAD}} \simeq 1.6 \times 10^{14}$ G and $M_{\text{fb}} \simeq 1.9 \times 10^{-3}M_\odot$. The modeling results for the XRT data are shown in Figure 3. For the magnetar radiation component, we have adopted a decay slope of 20 after the collapse according to the fitting results of Lü et al. (2015). It is shown that our model explains the afterglow data very well.

3.3 Further Model Test

In Subsection 3.1, we have found a sample of 12 short GRBs with an internal plateau. Three of them have high-quality

late X-ray data (GRB 070724A, GRB 101219A and GRB 160821B) while others show only one data point (GRB 120305A) or upper limits at $\sim 10^3 - 10^5$ s. The XRT light curves of the rest 9 GRBs with poor-quality late-time data are shown in Figure 4. For those without redshift measurements, an average redshift of 0.63 is assumed (Berger 2014). We note that, except GRB 120305A, all other bursts show no evidence of an extra component emerging after the sharp decay phase. However, even these upper limits are important for the consistency check of our model. To be self-consistent, the allowed parameter space of this model should be large enough to be compatible with these upper limits.

The most important parameters of our model are M_{fb} and $B_{\bullet, \text{MAD}}$, which, however, are highly uncertain. To compare the theoretical light curves with the data, we use a range of values of these two parameters while leave other parameters fixed. Specifically, we adopt $M_{\text{fb}} = 10^{-4} - 10^{-1} M_{\odot}$, $B_{\bullet, \text{MAD}} = 10^{11} - 10^{15}$ G, and fix $M_{\bullet} = 2.37 M_{\odot}$, $a_{\bullet} = 0.1$, $\eta_{\bullet, X}/f_{\bullet, b} = 1$ and $f_{\text{acc}} = 0.5$. We also assume a rest-frame collapse time $t_{\text{col}}/(1+z) = 100$ s. Using these parameters, we can calculate the theoretical light curves based on Equations (15), (16) and (20) and an assumed redshift of 0.63.

To show clearly in Figure 4, we simply consider three cases: (1) $M_{\text{fb}} = 0.01 M_{\odot}$, $B_{\bullet, \text{MAD}} = 10^{11} - 10^{15}$ G. The allowed luminosity regions are shown by two black boundary lines. We note that, as $B_{\bullet, \text{MAD}}$ increases, the light curve gradually changes from type I to type II; (2) $B_{\bullet, \text{MAD}} = 10^{14}$ G, $M_{\text{fb}} = 10^{-4} - 10^{-1} M_{\odot}$. The corresponding luminosity regions are shown by two red boundary lines. In this case, the pre-MAD magnetic field strength is high, leading to type II light curves, and more fall-back mass produces higher luminosity; (3) $B_{\bullet, \text{MAD}} = 10^{12}$ G, $M_{\text{fb}} = 10^{-4} - 10^{-1} M_{\odot}$. The allowed luminosity regions are exhibited by two green boundary lines. This case results in type I light curves. Since $\tilde{\tau}_{\text{MAD}} \propto M_{\text{fb}}^{3/5}$ while L_{preMAD} has no dependence on M_{fb} , more fall-back mass leads to longer plateau duration while leave the plateau luminosity constant. As shown in Figure 4, each case allows a large parameter space to be compatible with the data. It can also explain the late excess of GRB 120305A by simply adjusting some parameters (see the red solid line). Therefore, our model is further supported by the rest GRBs in our sample.

4 CONCLUSION AND DISCUSSION

Internal plateaus in GRB afterglows are commonly interpreted as the magnetic dipole emission from a supra-massive magnetar, and the sharp decay may imply the collapse of the magnetar to a BH. Fall-back accretion onto the new-born BH can produce long-lasting activities via the BZ process. The magnetic flux accumulated near the BH would be confined by the accretion disks for a period of time, resulting in roughly a constant BZ luminosity. As the accretion rate decreases, the magnetic flux is strong enough to obstruct gas infall and the MAD achieves. Then the BZ luminosity is determined by the instantaneous accretion rate (e.g., Tchekhovskoy & Giannios 2015). In the case of NS-NS mergers, we show that the BZ process could produce two types of typical X-ray light curves: type I shows a long-lasting late plateau, followed by a decay with slopes ranging from 5/3 to 40/9; type II exhibits roughly a single PL de-

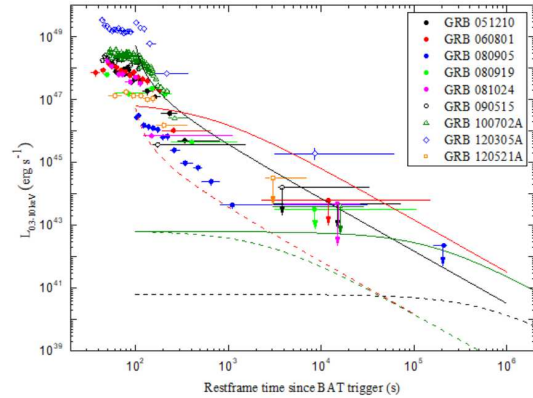


Figure 4. Compare our model with the rest GRB light curves in our sample. The data as shown are XRT luminosity light curves calculated in the observed 0.3–10 keV energy band. The lines are our theoretical light curves calculated with the following parameters: black solid line: $M_{\text{fb}} = 0.01 M_{\odot}$ and $B_{\bullet, \text{MAD}} = 10^{15}$ G; black dashed line: $M_{\text{fb}} = 0.01 M_{\odot}$ and $B_{\bullet, \text{MAD}} = 10^{11}$ G; red solid line: $B_{\bullet, \text{MAD}} = 10^{14}$ G and $M_{\text{fb}} = 0.1 M_{\odot}$; red dashed line: $B_{\bullet, \text{MAD}} = 10^{14}$ G and $M_{\text{fb}} = 10^{-4} M_{\odot}$; green solid line: $B_{\bullet, \text{MAD}} = 10^{12}$ G and $M_{\text{fb}} = 0.1 M_{\odot}$; green dashed line: $B_{\bullet, \text{MAD}} = 10^{12}$ G and $M_{\text{fb}} = 10^{-4} M_{\odot}$. For other parameters used, see the text for details.

decay with slope of 5/3. The light curve patterns are mostly determined by the magnetic field strength in the pre-MAD regime, and are weakly affected by the initial mass accretion rate or the total fall-back mass. Type I light curve requires low pre-MAD magnetic field strength, say, $B_{\bullet, \text{MAD}} \sim 10^{12}$ G, while type II corresponds to relatively high $B_{\bullet, \text{MAD}}$ values, say, $B_{\bullet, \text{MAD}} \sim 10^{14}$ G for typical parameters. We search for such signatures of the new-born BH from a sample of short GRBs with an internal plateau, and find two candidates: GRB 101219A and GRB 160821B, corresponding to type II and type I light curve, respectively. By comparing the theoretical light curves with their XRT data, we find our model can explain the data very well. The derived total fall-back mass $M_{\text{fb}} \sim 10^{-3} - 10^{-2} M_{\odot}$ is consistent with the results obtained from numerical simulations. For the rest bursts with poor-quality late X-ray data, our model are also compatible with observations.

Though the light curves of short GRBs with an internal plateau seem to support this scenario, the sample is too small, and more observations are needed to establish whether all such GRBs show light curves that are consistent with our model predictions. The first question is how to distinguish between this internal emission produced by the BZ process with the external afterglow component. Maybe the easiest way is to diagnose from the light curve. The external afterglow typically shows a PL decay with slope of ~ 1 , while the internal component exhibits either a long-lasting late plateau or a PL decay with slope of 5/3 or steeper. The late plateau component is more interesting. If the scenario of a collapsing supra-massive magnetar is preferred by an enlarged internal plateau sample in the future, the simultaneous observation of a late X-ray plateau (e.g., GRB 160821B) would be a further support for this framework. Besides, multi-band afterglow observations could serve as an auxiliary diagnosis since the standard afterglow models have definite predictions to the afterglow evolutions. Finally,

we emphasize that the BH emission could, in principle, not be seen due to the following two reasons: first, this emission could be hidden by the external afterglow component; second, if the fall-back process is inefficient, the BH emission could be intrinsically weak and below the detection limit. For the latter, as stated in Section 2, the magnetar accretion and propeller processes could greatly decrease the fall-back mass. Outflows from the accretion disk could also interact with the fall-back material and reduce the BH emission (Fernández et al. 2015).

It should be noted that the luminosity evolution in the MAD state and the value of M_{fb} are strongly dependent on the mass accretion rate, which was assumed to be a fraction of the fall-back accretion rate in this work. For example, if we assume \dot{M} scales with $\dot{M} \propto t^{-4/3}$, the decay slope of the MAD luminosity would be different from 5/3, and the value of M_{fb} would be an order of magnitude smaller than the results obtained in Section 3 (Kisaka, Ioka & Sakamoto 2017). Besides, we did not consider the BH evolution during the accretion and BZ processes, which can in principle affect the BH mass M_{\bullet} and spin parameter a_{\bullet} (e.g., Chen et al. 2017; Lei et al. 2017). However, for very low accretion rate as studied in this work, this effect might be ignored. From another point of view, some sacrifice in accuracy may be justified, given that some related physical processes (e.g., the accretion and propeller processes, the GW effect and the interaction between outflows and fall-back matter) were not taken into account in our model. Finally, it is interesting to further investigate why type I and type II light curves correspond to much different pre-MAD magnetic field strength, which is beyond the scope of this work.

Kisaka & Ioka (2015) employed the same BZ process to interpret the extended emission of short GRBs and their X-ray afterglows. Considering that the internal plateau and extended emission have similar durations and continuous luminosity distribution (Lü et al. 2015), their model can also explain the light curve of GRB 160821B-like bursts (Kisaka, Ioka & Sakamoto 2017). We emphasize that our model is different from theirs on three points: (1) different central engines. We assume the product of the NS-NS merger is a supra-massive magnetar which collapses to a BH at late times, while their assumed central engine is a prompt BH; (2) different theoretically light curves. Our model predicts two types of typical X-ray light curves, while theirs can only produce the one with a plateau followed by a steep decay, corresponding to our type I light curve. It is easy to understand. Our type II light curve is intrinsically due to the zero point effect, which changes the zero point from the beginning time of the BH accretion to the burst trigger time. While there is no such transformation in the case of a prompt BH central engine; (3) on the maximum decay slope after the internal plateau. Their model predicts a maximum slope of 40/9, while ours can produce a much steeper decay. Some internal plateaus followed by a decay with slope as steep as ~ 10 seem to support the magnetar collapse scenario (e.g., Rowlinson et al. 2013; Lü et al. 2015).

The two scenarios can, in principle, be distinguished by observations. As the supra-massive magnetar collapses, the magnetic field would be ejected as the event horizon swallows the star based on the ‘no-hair theorem’. The entire magnetic field outside the horizon detaches and reconnects, resulting in intense electromagnetic emission in a

short time (Baumgarte & Shapiro 2003; Lehner et al. 2012; Dionysopoulou et al. 2013). One such product is a bright radio ‘blitzar’, which was proposed as a likely source of fast radio bursts (FRB; Falcke & Rezzolla 2014). This FRB-like event, if observed at the end of the internal plateau, can be an evidence of the collapse of a supra-massive magnetar to a BH (Zhang 2014).

Our model has two important implications:

First, considering the similarity of the internal plateau and extended emission of short GRBs, our model may have the potential to explain the extended emission and the X-ray afterglows. Within the magnetar scenario, the spin-down process with or without a significant accretion was investigated to explain the extended emission (Metzger, Quataert & Thompson 2008; Bucciantini et al. 2012; Gompertz, O’Brien & Wynn 2014). The magnetar might collapse at some time, then the X-ray afterglow could be interpreted as the radiation from the BZ process of the new-born BH. Interestingly, most of the afterglow light curves can be best fit by a single PL (Lü et al. 2015), while only a minority show a long-lasting plateau (e.g., GRB 060614). These features seem to resemble our theoretical light curves. This issue will be studied in future work.

Second, as suggested by Kisaka & Ioka (2015), the long-lasting activities of the new-born BH would significantly affect the macronovae. Macronovae could be powered by the radioactivity of r-process elements synthesized in the ejecta of a NS-NS merger (e.g., Li & Paczyński 1998; Kulkarni 2005; Metzger et al. 2010; Barnes & Kasen 2013), or by the energy injection from the central engine, e.g., a BH or a stable magnetar (e.g., Yu, Zhang & Gao 2013; Metzger & Piro 2014; Gao et al. 2015; Kisaka, Ioka & Takami 2015; Kisaka, Ioka & Nakar 2016). Recently, Kisaka, Ioka & Nakar (2016) proposed a X-ray powered model in which the X-ray excess (e.g., GRB 130603B; Fong et al. 2014) gives rise to the simultaneously observed infrared excess via thermal re-emission. However, their model did not specify the mechanism of the X-ray excess. Our model provides a possible mechanism for such kind of X-ray excess, and the X-ray powered macronovae will be further studied in a separated paper.

In our model, the late X-ray afterglows of short GRBs with an internal plateau are produced by the BZ process of a new-born Kerr BH, the magnetic field of which is supported by the surrounding disk. Recently, Nathanail, Most & Rezzolla (2017) showed that the collapse of a rotating magnetized NS would leave behind a charged spinning (Kerr-Newman) BH. Such a charged BH was also proposed by Zhang (2016) as a product of BH-BH mergers, of which at least one carries a certain amount of charge (see also Liebling & Palenzuela 2016). In our study, if the product of collapsing supra-massive NS is a Kerr-Newman BH, then the BZ power can be provided by the BH itself even if there is no fall-back accretion. A quantitative comparison between this model and ours is interesting, which is beyond the scope of this work.

ACKNOWLEDGEMENTS

We acknowledge the anonymous referee for helpful comments and suggestions. We also thank Bing Zhang and He

Gao for helpful discussions. This work made use of data supplied by the UK Swift Science Data Centre at the University of Leicester. This study was supported by the Strategic Priority Research Program of the Chinese Academy of Sciences (Grant No. XDB23040400). S. L. Xiong was also supported by the Hundred Talents Program of the Chinese Academy of Sciences (Grant No. Y629113). W. H. Lei and W. Chen acknowledge support from the National Natural Science Foundation of China (Grant U1431124). B. B. Zhang acknowledges support from the Spanish Ministry Projects AYA2012-39727-C03-01 and AYA201571718-R. L. M. Song acknowledges support from the National Program on Key Research and Development Project (Grant No. 2016YFA0400801) and the National Basic Research Program of China (Grant No. 2014CB845802).

REFERENCES

- Antoniadis J. et al., 2013, *Science*, 340, 1233232
- Baiotti L., De Pietri R., Manca G. M., Rezzolla L., 2007, *Phys. Rev. D*, 75, 044023
- Barnes J., Kasen D., 2013, *ApJ*, 775, 18
- Barthelmy S. D. et al., 2005a, *Space Sci. Rev.*, 120, 143
- Barthelmy S. D. et al., 2005b, *Nature*, 438, 994
- Baumgarte T. w., Shapiro S., 2003, *ApJ*, 585, 930
- Berger E., 2014, *ARA&A*, 52, 43
- Berger E., et al., 2005, *Nature*, 438, 988
- Berger E., Cenko S. B., Fox D. B., Cucchiara A., 2009, *ApJ*, 704, 877
- Bisnovatyi-Kogan G. S., Ruzmaikin A. A., 1974, *ApJS*, 28, 45
- Bisnovatyi-Kogan G. S., Ruzmaikin A. A., 1976, *ApJS*, 42, 401
- Blandford R. D., Znajek R. L., 1977, *MNRAS*, 179, 433
- Breeveld A. A., Siegel M. H., 2016, *GCN*, 19839, 1
- Bucciantini N., Metzger B. D., Thompson T. A., Quataert, E., 2012, *MNRAS*, 419, 1537
- Burrows D. N., et al., 2005, *Space Sci. Rev.*, 120, 165
- Campana S., et al., 2006, *A&A*, 454, 113
- Chen W. X., Beloborodov A. M., 2007, *ApJ*, 657, 383
- Chen W., Xie W., Lei W. H., Zou Y. C., Lü H. J., Liang E. W., Gao H., Wang D. X., 2017, *ApJ*, 849, 119
- Chevalier R. A., Li Z. Y., 2000, *ApJ*, 536, 195
- Chornock R., Berger E., 2010, *GCN*, 11518, 1
- Ciolfi R., Kastaun W., Giacomazzo B., Endrizzi A., Siegel D. M., Perna R., 2017, *Phys. Rev. D*, 95, 063016
- Corsi A., Mészáros P., 2009, *ApJ*, 702, 1171
- Covino S., Palazzi E., 2010, *GCN*, 11463, 1
- Dai Z. G., Wang X. Y., Wu X. F., Zhang B., 2006, *Science*, 311, 1127
- Dall’Osso S., Giacomazzo B., Perna R., Stella L., 2015, *ApJ*, 798, 25
- Demorest P. B., Pennucci T., Ransom S. M., Roberts M. S. E., Hessels J. W. T., 2010, *Nature*, 467, 1081
- De Pasquale M., et al., 2016, *MNRAS*, 455, 1027
- Dermer C. D., 2004, *ApJ*, 614, 284
- Di Matteo T., Perna R., Narayan R., 2002, *ApJ*, 579, 706
- Dionysopoulou K., Alic D., Palenzuela C., Rezzolla L., Giacomazzo B., 2013, *Phys. Rev. D*, 88, 044020
- Doneva D. D., Kokkotas K. D., Pnigouras P., 2015, *Phys. Rev. D*, 92, 104040
- Eichler D., Livio M., Piran T., Schramm D. N., 1989, *Nature*, 340, 126
- Evans P. A., et al., 2007, *A&A*, 469, 379
- Evans P. A., et al., 2009, *MNRAS*, 397, 1177
- Evans P. A., Goad M. R., Osborne J. P., Beardmore A. P., 2016, *GCN*, 19837, 1
- Falcke H., Rezzolla L., 2014, *A&A*, 562, A137
- Fan Y. Z., Wu X. F., Wei D. M., 2013, *Phys. Rev. D*, 88, 067304
- Fenimore E. E., Madras C. D., Nayakshin S., 1996, *ApJ*, 473, 998
- Fernández R., Quataert E., Schwab J., Kasen D., Rosswog S., 2015, *MNRAS*, 449, 390
- Fong W., Berger E., Fox D. B., 2010, *ApJ*, 708, 9
- Fong W., et al., 2013, *ApJ*, 769, 56
- Fong W., et al., 2014, *ApJ*, 780, 118
- Fox D. B., et al., 2005, *Nature*, 437, 845
- Gao H., Ding X., Wu X. F., Dai Z. G., Zhang B., 2015, *ApJ*, 807, 163
- Gao H., Zhang B., Lü H. J., 2016, *Phys. Rev. D*, 93, 044065
- Gao H., Cao Z. J., Zhang, B., 2017, *ApJ*, 844, 112
- Gao W. H., Fan Y. Z., 2006, *Chinese J. Astron. Astrophys.*, 6, 513
- Gehrels N., et al., 2005, *Nature*, 437, 851
- Gelbord J. M., et al., 2010, *GCN*, 11461, 1
- Giacomazzo B., Perna R. 2013, *ApJ*, 771, L26
- Gibson S. L., Wynn G. A., Gompertz B. P., O’Brien P. T., 2017, *MNRAS*, 470, 4925
- Golenetskii S., et al., 2010, *GCN*, 11470, 1
- Gompertz B. P., O’Brien P. T., Wynn G. A., 2014, *MNRAS*, 438, 240
- Gompertz B. P., O’Brien P. T., Wynn G. A., Rowlinson A., 2013, *MNRAS*, 431, 1745
- Gu W. M., Liu T., Lu J. F., 2006, *ApJ*, 643, L87
- Hebeler K., Lattimer J. M., Pethick C. J., Schwenk A., 2013, *ApJ*, 773, 11
- Hotokezaka K., Kiuchi K., Kyutoku K., Okawa H., Sekiguchi Y.-I., Shibata M., Taniguchi K., 2013, *Phys. Rev. D*, 88, 044026
- Igumenshchev I. V., Narayan R., Abramowicz M. A., 2003, *ApJ*, 592, 1042
- Janiuk A., Yuan Y., Perna R., Di Matteo T., 2007, *ApJ*, 664, 1011
- Jarosik N., et al., 2011, *ApJS*, 192, 14
- Kann D. A., et al., 2011, *ApJ*, 734, 96
- Kasliwal M. M., Korobkin O., Lau R. M., Wollaeger R., Fryer C. L., 2017, *ApJ*, 834, L34
- Kisaka S., Ioka K., 2015, *ApJ*, 804, L16
- Kisaka S., Ioka K., Takami H., 2015, *ApJ*, 802, 119
- Kisaka S., Ioka K., Nakar E., 2016, *ApJ*, 818, 104
- Kisaka S., Ioka K., Sakamoto T., 2017, *ApJ*, 846, 142
- Kiuchi K., Sekiguchi Y., Shibata M., Taniguchi K., 2009, *Phys. Rev. D*, 80, 064037
- Kocevski D., et al., 2010, *MNRAS*, 404, 963
- Kouveliotou C., Meegan C. A., Fishman G. J., Bhat N. P., Briggs M. S., Koshut, T. M., Paciesas W. S., Pendleton G. N., 1993, *ApJ*, 413, L101
- Krimm H. A., et al., 2010, *GCN*, 11467, 1
- Kuin N. P. M., Gelbord J. M., 2010, *GCN*, 11472, 1
- Kulkarni S. R., 2005, preprint (arXiv: astro-ph/0510256)
- Kumar P., Panaitescu A., 2000, *ApJ*, 541, L51
- Kumar P., Zhang B., 2015, *Phys. Rep.*, 561, 1
- Lasky P. D., Glampedakis K., 2016, *MNRAS*, 458, 1660
- Lasky P. D., Haskell B., Ravi V., Howell E. J., Coward D. M., 2014, *Phys. Rev. D*, 89, 047302
- Lee W. H., Ramirez-Ruiz E., López-Cámara D., 2009, *ApJ*, 699, L93
- Lee H. K., Wijers R. A. M. J., Brown G. E., 2000, *Phys. Rep.*, 325, 83
- Lehner L., Palenzuela C., Liebling S. L., Thompson C., Hanna C., 2012, *Phys. Rev. D*, 86, 104035
- Lei W. H., Zhang B., 2011, *ApJ*, 740, L27
- Lei W. H., Wang D. X., Ma R. Y., 2005, *ApJ*, 619, 420
- Lei W. H., Wang D. X., Zhang L., Gan Z. M., Zou Y. C., Xie Y., 2009, *ApJ*, 700, 1970
- Lei W. H., Zhang B., Liang E. W., 2013, *ApJ*, 765, 125
- Lei W. H., Zhang B., Wu X. F., Liang E. W., 2017, *ApJ*, 849, 47

- Levan A. J., Wiersema K., Tanvir N. R., Malesani D., Xu D., de Ugarte Postigo A., 2016, *GCN*, 19846, 1
- Li L. X., 2000, *Phys. Rev. D*, 61, 084016
- Li L. X., Paczyński B., 1998, *ApJ*, 507, L59
- Li A., Zhang B., Zhang N. B., Gao H., Qi B., Liu T., 2016, *Phys. Rev. D*, 94, 083010
- Liang E. W., Zhang B. B., Zhang B., 2007, *ApJ*, 670, 565
- Liebling S. L., Palenzuela C., 2016, *Phys. Rev. D*, 94, 064046
- Liu T., Hou S. J., Xue L., Gu, W. M., 2015, *ApJS*, 218, 12
- Lü H. J., Zhang B., 2014, *ApJ*, 785, 74
- Lü H. J., Zhang B., Lei W. H., Lasky P. D., 2015, *ApJ*, 805, 89
- Lü H. J., Zhang H. M., Zhong S. Q., Hou S. J., Sun H., Rice J., Liang E. W., 2017, *ApJ*, 835, 181
- Lyford N. D., Baumgarte T. W., Shapiro S. L., 2003, *ApJ*, 583, 410
- Lyons, N., O'Brien, P. T., Zhang, B., Willingale R., Troja E., Starling R. L. C., 2010, *MNRAS*, 402, 705
- Margalit B., Metzger B. D., Beloborodov A. M., 2015, *Phys. Rev. Lett.*, 115, 171101
- Margutti R., et al., 2011, *MNRAS*, 417, 2144
- McKinney J. C., 2005, *ApJ*, 630, L5
- Metzger B. D., Piro A. L., 2014, *MNRAS*, 439, 3916
- Metzger B. D., Piro A. L., Quataert E., 2008, *MNRAS*, 390, 781
- Metzger B. D., Quataert E., Thompson T. A., 2008, *MNRAS*, 385, 1455
- Metzger B. D., et al., 2010, *MNRAS*, 406, 2650
- Narayan R., Paczynski B., Piran T., 1992, *ApJ*, 395, L83
- Narayan R., Piran T., Kumar P., 2001, *ApJ*, 557, 949
- Narayan R., Igumenshchev I. V., Abramowicz M. A., 2003, *PASJ*, 55, L69
- Nathanail A., Most E. R., Rezzolla L., 2017, *MNRAS*, 469, L31
- Norris J. P., Bonnell J. T., 2006, *ApJ*, 643, 266
- Paczynski B., 1991, *Acta Astron.*, 41, 257
- Palmer D. M., et al., 2016, *GCN*, 19844, 1
- Pandey S. B., Zheng W., Rujopakarn W., 2010, *GCN*, 11462, 1
- Piro A. L., Ott C., 2011, *ApJ*, 736, 108
- Popham R., Woosley S. E., Fryer C., 1999, *ApJ*, 518, 356
- Ravi V., Lasky P. D., 2014, *MNRAS*, 441, 2433
- Rezzolla L., Giacomazzo B., Baiotti L., Granot J., Kouveliotou C., Aloy M. A., 2011, *ApJ*, 732, L6
- Roming P. W. A., et al., 2005, *Space Sci. Rev.*, 120, 95
- Rossi E. M., Begelman M. C., 2009, *MNRAS*, 392, 1451
- Rosswog S., 2007, *MNRAS*, 376, L48
- Rosswog S., Davies M. B., 2002, *MNRAS*, 334, 481
- Rosswog S., Piran T., Nakar E., 2013, *MNRAS*, 430, 2585
- Rowlinson A., et al., 2010, *MNRAS*, 409, 531
- Rowlinson A., O'Brien P. T., Metzger B. D., Tanvir N. R., Levan A. J., 2013, *MNRAS*, 430, 1061
- Sari R., Piran T., Narayan R., 1998, *ApJ*, 497, L17
- Siegel, M. H., Barthelmy, S. D., Burrows, D. N., Lien A. Y., Marshall F. E., Palmer D. M., Sbarufatti B., 2016, *GCN*, 19833, 1
- Stanbro M., Meegan C., 2016, *GCN*, 19843, 1
- Stergioulas N., Friedman J. L., 1995, *ApJ*, 444, 306
- Tchekhovskoy A., & Giannios D., 2015, *MNRAS*, 447, 327
- Tchekhovskoy A., Narayan R., McKinney J. C., 2010, *ApJ*, 711, 50
- Tchekhovskoy A., Narayan R., McKinney J. C., 2011, *MNRAS*, 418, L79
- Tchekhovskoy A., Metzger B. D., Giannios D., Kelley L. Z., 2014, *MNRAS*, 437, 2744
- Tchekhovskoy A., 2015, in Contopoulos, G. et al., eds, *Astrophysics and Space Science Library*, Vol. 414, *The Formation and Disruption of Black Hole Jets*. Springer, Switzerland, p.45
- Troja E., et al., 2007, *ApJ*, 665, 599
- Troja E., et al., 2016, *GCN*, 20222, 1
- Wang D. X., Xiao K., Lei W. H., 2002, *MNRAS*, 335, 655
- Xie W., Lei W. H., Wang D. X., 2016, *ApJ*, 833, 129
- Yu Y. W., Zhang B., Gao, H., 2013, *ApJ*, 776, L40
- Zamaninasab M., Clausen-Brown E., Savolainen T., Tchekhovskoy A., 2014, *Nature*, 510, 126
- Zhang B., 2013, *ApJ*, 763, L22
- Zhang B., 2014, *ApJ*, 780, L21
- Zhang B., 2016, *ApJ*, 827, L31
- Zhang B., Mészáros P., 2001, *ApJ*, 552, L35
- Zhang B. B., Zhang B., Liang E. W., Wang X. Y., 2009, *ApJ*, 690, L10
- Zhang Q., Huang Y. F., Zong H. S., 2016, *ApJ*, 823, 156
- Ziaeepour H., Barthelmy S. D., Parsons A., Page K. L., de Pasquale M., Schady P., 2007, *GCNR*, 74, 2

This paper has been typeset from a $\text{\TeX}/\text{\LaTeX}$ file prepared by the author.